Multiple Scattering X-Ray Absorption Studies of Zn^{2+} Binding Sites in Bacterial Photosynthetic Reaction Centers

Lisa Giachini,*† Francesco Francia,‡ Antonia Mallardi,§ Gerardo Palazzo,¶ Emilio Carpenè,‖ Federico Boscherini,*† and Giovanni Venturoli†‡

*Dipartimento di Fisica, Università di Bologna, Bologna, Italy; †Istituto Nazionale per la Fisica della Materia (INFM), UdR di Bologna, Bologna, Italy; ‡Laboratorio di Biochimica e Biofisica, Dipartimento di Biologia, Università di Bologna, Bologna, Italy; §Istituto per i Processi Chimico-Fisici, CNR, Bari, Italy; ¶Dipartimento di Chimica, Università di Bari, Bari; and ‖Dipartimento di Biochimica, Sezione Biochimica Veterinaria, Università di Bologna, Ozzano Emilia, Bologna, Italy

ABSTRACT Binding of transition metal ions to the reaction center (RC) protein of the photosynthetic bacterium *Rhodobacter sphaeroides* has been previously shown to slow light-induced electron and proton transfer to the secondary quinone acceptor molecule, Q_B. On the basis of x-ray diffraction at 2.5 Å resolution a site, formed by AspH124, HisH126, and HisH128, has been identified at the protein surface which binds Cd^{2+} or Zn^{2+}. Using Zn K-edge x-ray absorption fine structure spectroscopy we report here on the local structure of Zn^{2+} ions bound to purified RC complexes embedded into polyvinyl alcohol films. X-ray absorption fine structure data were analyzed by combining ab initio simulations and multiparameter fitting; structural contributions up to the fourth coordination shell and multiple scattering paths (involving three atoms) have been included. Results for complexes characterized by a Zn to RC stoichiometry close to one indicate that Zn^{2+} binds two O and two N atoms in the first coordination shell. Higher shell contributions are consistent with a binding cluster formed by two His, one Asp residue, and a water molecule. Analysis of complexes characterized by ~2 Zn ions per RC reveals a second structurally distinct binding site, involving one O and three N atoms, not belonging to a His residue. The local structure obtained for the higher affinity site nicely fits the coordination geometry proposed on the basis of x-ray diffraction data, but detects a significant contraction of the first shell. Two possible locations of the second new binding site at the cytoplasmic surface of the RC are proposed.

INTRODUCTION

The bacterial photosynthetic reaction center (RC) is a membrane-bound pigment-protein complex that initiates the conversion of light into chemical energy. It catalyzes a series of light-driven electron and proton transfer reactions resulting in the formation across the bacterial membrane of a proton gradient utilized for ATP synthesis (Okamura et al., 2000). In the RC of *Rhodobacter sphaeroides*, after absorption of a photon, electron transfer proceeds from the first excited singlet state of the primary donor P (a bacteriochlorophyll dimer) through a series of intermediate acceptors (a bacteriopheophytin and a primary quinone acceptor Q_A) to a loosely bound secondary quinone Q_B, yielding the membrane-spanning charge separated state $P^+Q_B^-$. Upon re-reduction of P^+ by its physiological electron donor (a soluble cytochrome c_2), a new photoexcitation of P leads to the full reduction and protonation of Q_B^- to QH_2, which dissociates from the Q_B site and acts as a mobile electron and proton carrier from the RC to the bc_1 complex (Crofts and Wraight, 1983; Feher et al., 1989; Gunner, 1991; Okamura et al., 2000).

During the last decades the RC from *Rb. sphaeroides* has been the subject of an impressive number of spectroscopic investigations which provided a detailed thermodynamic and kinetic characterization of electron and proton transfer processes (Woodbury and Allen, 1995; Hoff and Deisenhofer, 1997; Okamura et al., 2000). The availability of site-directed mutants and of x-ray diffraction (XRD) data at atomic resolution (Allen et al., 1986, 1987a,b; Ermler et al., 1994) has made the RC from *Rb. sphaeroides* an ideal system for exploring the basic structure-function relationships that govern biological electron and proton transfer. Two challenging aspects are intensively investigated by exploiting the RC as a model: the nature of the conformational protein dynamics coupled to electron transfer; and the role of specific amino acids or local protein environments in influencing electron and proton transfer (see e.g., Paddock et al., 1990; Takahashi and Wraight, 1992; McMahon et al., 1998; Balabin and Onuchic, 2000; Poluektov et al., 2003; Baxter et al., 2004).

Recently, elucidation of these issues has taken advantage of the discovery that binding of metal ions (Zn^{2+} and Cd^{2+}) to the RC affects the rate of specific electron and proton transfer processes. Utschig et al. (1998) have shown that Zn^{2+} binds to the RC in a site distinct from the Fe site, the only one constitutive transition metal ion site of the RC, located between the Q_A and Q_B acceptors. Upon binding of Zn^{2+} the transfer of the first electron from Q_A^- to Q_B is slowed and the room-temperature kinetics become distributed over the microsecond to millisecond time scale. This observation has suggested that Zn^{2+} acts by limiting protein local motions important for rapid electron transfer (Utschig et al., 1998). Paddock et al. (1999) confirmed and extended

Submitted August 3, 2004, and accepted for publication December 15, 2004.

Address reprint requests to Giovanni Venturoli, E-mail: ventur@alma.unibo.it.

0006-3495/05/03/2038/09 $2.00

doi: 10.1529/biophysj.104.050971

these results, demonstrating that Zn^{2+} and Cd^{2+} binding decreases by more than one order of magnitude the rate constant of the proton-assisted second electron transfer, i.e., the reaction $Q_A^- Q_B^- + H^+ \rightarrow Q_A(Q_BH)^-$. In the presence of Zn^{2+} and Cd^{2+} the rate of proton transfer is slowed by a factor $>10^2$ and becomes the rate-limiting step (Paddock et al., 1999; Gerencsér and Maroti, 2001).

Axelrod et al. (2000) have determined the binding site of Zn^{2+} in the RC using XRD at 2.5 Å resolution. They found that the metal ion site is located ~20 Å from the Q_B site at the cytoplasmic surface of the RC. Bound to the Zn are the imidazole side chains of two histidines (HisH126, HisH128) and the side chain of an aspartic acid (AspH124). The most significant structural difference between the RC with and without a bound metal ion is the positions of the side-chain ligands. Both histidines appear to undergo side-chain conformational changes that enable them to bind to the metal ions via the N^{δ} atoms of the imidazole ring. One of the oxygens of the side chain of AspH124 is also coordinated to the metal ion. In addition to the three amino acidic residues a water molecule was also proposed to interact with the Zn^{2+} suggesting tetrahedral coordination, which is the predominant geometry found in Zn^{2+} containing proteins. XRD data indicate that Cd^{2+} binding involves the same cluster of residues and possibly three water molecules in an octahedral coordination geometry.

The location of this binding site has opened the way to a series of studies, which contributed significantly to identify the dominant proton pathway connecting the protein surface to Q_B. By combining site-directed mutagenesis and reversible binding of Zn^{2+} and Cd^{2+} it was shown that: a), HisH126 and HisH128 are involved in the pathway of the first proton to Q_B^- at the entry point (Paddock et al., 1999; Ädelroth et al., 2001); b), proton transfer proceeds through AspM17 and AspL210 (Paddock et al., 2000); and c), the second proton supplied to $(Q_BH)^-$ by GluL212 and leading to the formation of quinol share the same entry point of the first proton, close to the metal binding cluster AspH124, HisH126, and HisH128 (Ädelroth et al., 2000). By examining the pH dependence of Cd^{2+} binding in native and in mutant RCs that lack the imidazole group of HisH126 or HisH128 Paddock et al. (2003) concluded that inhibition of proton transfer by the metal ion is predominantly a consequence of competition with protons for binding to HisH126 and HisH128, thus hampering the function of these residues as proton donor/acceptors along the proton pathway to the Q_B site. This study allowed determination of the proton affinities (i.e., pK_A values) of the histidines, a parameter of fundamental importance for the proton transfer processes.

The studies summarized above show that metal ion binding to the RC is a powerful tool in elucidating subtle aspects of electron and proton transfer. The local structure of the bound metal ions is expected to carry valuable information that can be profitably used to elucidate the details of the inhibition mechanisms. For these reasons we undertook x-ray absorption fine structure (XAFS) spectroscopy studies of Zn^{2+} binding site(s) in noncrystallized purified Zn-RC complexes.

XAFS (Koninsgsberger and Prins, 1988) is an ideal tool for selectively probing the local structure of a metal ion in a protein. XAFS obtains local structural information from the analysis of the modulations in the photoelectric absorption cross section, which occur above a core level absorption edge, yielding a quantitative measurement of the local structure in the first few coordination shells. Especially when the scattering atoms have a low atomic number, as in the field of biomolecules, the inclusion of multiple scattering (MS) contributions in the analysis of the XAFS can be required and can in fact provide information which is essential in order to allow the identification of the amino acidic residues coordinated to the metal, as indicated by Strange et al. (1987). The continuous development of advanced data simulation and analysis programs, which are able to treat MS contributions to the XAFS spectra (Filipponi et al., 1995; Ankudinov et al., 1998; Rehr and Albers, 2000), has significantly improved the reliability of the technique. Although the early studies concentrated on methodological aspects (existence and importance of MS), recent progress allows using MS as a structural tool (see e.g., Meneghini and Morante, 1998).

In the field of metalloproteins one important advantage of XAFS is that it is applicable to noncrystallized samples. Moreover, it can be usefully combined with x-ray diffraction to significantly improve the accuracy of the determination of the interatomic distances, which can be determined typically within a few hundredths of an Å for the first shell. Both these aspects are important for our investigation of Zn^{2+} binding site(s). We recall that the Fe site geometry in the RC has been previously studied by Eisenberger et al. (1982), Bunker et al. (1982), and recently by Chen et al. (2004). For recent reviews of the application of XAS to metalloproteins, see Samar Hasnain and Hodgson (1999) and Samar Hasnain and Strange (2003).

In this article, we report an XAFS analysis of Zn-RC complexes characterized by different Zn^{2+} to RC stoichiometries embedded in polyvinyl alcohol (PVA) films. Our data define the local structure of the high affinity site located by XRD and reveal a second structurally distinct binding site, involving three N atoms and one O atom.

MATERIALS AND METHODS

Reaction centers were purified from *Rb. Sphaeroides R26* according to Gray et al. (1990). The concentration of RCs was measured spectrophotometrically by the absorbance at 802 nm, using an extinction coefficient $\varepsilon_{802} = 288$ mM^{-1} cm^{-1} (Straley et al., 1973). The amounts of Zn and Fe bound to the RC were determined by atomic absorption spectroscopy using an Instrumentation Laboratories (Lexington, MA) IL S11 model spectrophotometer. Analysis for Fe content of the examined preparations yielded a Fe/RC ratio of 0.9 ± 0.1, consistent with one Fe site per RC. As a consequence essentially coincident Zn/RC stoichiometries were obtained when RC was evaluated spectrophotometrically or on the basis of Fe content. In agreement

with Utschig et al. (1998) we found that purified RCs, without any incubation in Zn containing buffers, were characterized by a Zn/RC molar ratio of ~0.15.

RC-Zn complexes were prepared using essentially the procedures described by Utschig et al. (1998), which consist in incubating the RC suspension with stoichiometric excess of Zn^{2+} followed by size exclusion chromatography to separate the free metal ion from the Zn-RC complexes. By incubating the RC with different equivalents of $ZnSO_4$ per RC followed by an appropriate gel filtration chromatography protocol (see below) we could systematically obtain RC-Zn complexes containing ~1 or 2 Zn^{2+} per RC. To prepare samples characterized by a Zn^{2+}/RC ratio close to 2, 1 mL suspension of 90 μM RC was incubated for 15 h at ice temperature with a four-time excess of $ZnSO_4$ in 10 mM Tris buffer, pH 7.9, containing 0.045% LDAO and 280 mM NaCl. At the end of the incubation time, the sample was sequentially eluted through two Sephadex G25 (Pharmacia, Uppsala, Sweden) columns (1cm diameter × 15 cm and 0.5 cm diameter × 20 cm, respectively) equilibrated with 0.045% LDAO, 50 mM NaCl, 10 mM Tris pH 7.9. EDTA was additionally present at 10 μM only in the first column. Metal analysis of three independent preparations yielded average values of 2.4 ± 0.2 and 1.8 ± 0.2 Zn/RC in the protein fractions collected after the first and the second column respectively, with 0.2 being the standard deviation between the different sample preparations. Good separation between free and RC-bound Zn^{2+} was indicated by column elution profiles, which exhibited two distinctly separated Zn^{2+} peaks, in agreement with Utschig et al. (1998).

The reversibility of Zn^{2+} binding was tested by dialysis of RC-Zn complexes prepared as described above against the metal chelating resin Chelex 100. When samples, characterized by Zn/RC ≅ 2 were dialyzed for 5 h against 100-volume of 0.045% LDAO, 10μM EDTA, 10 mM Tris pH 7.9 containing 5 g of Chelex 100 metal-chelating resin (Bio-Rad, Hercules, CA, 100-200 mesh Na form) and for 5 h against 200-volume of 0.045% LDAO, 50 mM NaCl, 10 mM Tris pH 7.9, Zn/RC stoichiometry was not reduced appreciably. However, when the first dialysis step was prolonged to 48 h, the Zn^{2+} content was reduced to levels lower than 0.2 Zn^{2+}/RC, similarly to what observed by Utschig et al. (1998) for RC-Zn complexes characterized by 1.0 ± 0.2 Zn/RC.

These measurements strongly suggests that at least one additional Zn binding site is present in the RC besides the high affinity one documented in the literature. The existence of a second, lower affinity, Zn^{2+} binding site, is corroborated by the observation that a RC-Zn^{2+} complex characterized by 1.8 Zn/RC could be obtained following the above described procedure under different incubation conditions, i.e., at overall RC and $ZnSO_4$ concentrations in the incubation medium decreased by a factor of five. We note that these concentrations (18 μM RC and 72 μM $ZnSO_4$) are a factor of two lower than those used by Utschig et al. (1998) to prepare stoichiometric RC-Zn complexes. Samples characterized by Zn/RC ratios close to 1 were obtained essentially following the same procedure except that RCs were incubated in the presence of 1.2 equivalents of $ZnSO_4$.

Utschig et al. (1998) have shown that stoichiometric binding of Zn does not displace the buried Fe constitutively bound to the RC. We routinely determined the Fe content of our preparations by absorption spectroscopy and always found Fe/RC ratios very close to one, both in native RCs (containing low amounts of Zn (<0.2 Zn/RC)) and in Zn-RC complexes characterized by ~2 Zn/RC. This confirms the conclusion of Utschig et al. (1998) and also indicates that binding of two Zn metal ions per RC does not interfere with Fe binding.

Two samples were analyzed by XAFS, characterized by 1.9 and 0.9 Zn/RC, hereafter named sample 1 and sample 2, respectively.

Zn-RC containing PVA films were prepared by supplementing the Zn-RC suspension described above with 2.5% w/v PVA (Fluka, Buchs, Switzerland, $M_w \approx 130000$). The final RC concentration was typically 20–30 μM. To form the film, the suspension was dehydrated under dry N_2 flow for ~5 h. Further dehydration was obtained under vacuum. Zinc 3,5-heptanedionate (Lancaster, Morecambe, UK), Zinc 5,10,15,20-tetra(4-pyridyl) −21*H*, 23*H*-porphine and zinc phthalocyanine (Aldrich, Milwaukee, WI) were used as reference compounds.

Zn K-edge XAFS measurements were performed at the BM 8 ''GILDA'' beam-line of the European Synchrotron Radiation Facility (ESRF) in Grenoble, France. An Si(311) double crystal monochromator employing dynamical sagittal focusing (Pascarelli et al., 1996) was used; the photon flux was of the order of 5×10^{10} photons per second and the spot size was $\sim 1 \times 1$ mm^2. Harmonics were rejected using a pair of grazing incidence Pd-coated mirrors. The energy dependence of the Zn absorption coefficient was monitored by measuring the intensity of the Zn K_α fluorescence, using a 13-element hyper-pure Ge detector equipped with fast digital electronics with a peaking time equal to 1 μs (Ciatto et al., 2004).

Samples were measured at both room and liquid nitrogen temperature, yielding virtually identical results. The data analyzed are the average of four spectra taken with an integration time of 30 s/point. The presence of time-dependent shifts in the absorption threshold energy, linked to radiation induced reduction, was explicitly checked and was ruled out.

RESULTS AND DISCUSSION

Data analysis and model compounds

Together with the two samples described above, XAFS spectra of three Zn containing molecules of known structure, in which Zn is present in a local coordination similar to that expected in the RC, were measured. As mentioned above, XRD data at 2.5 Å resolution (Axelrod et al., 2000) have identified a Zn^{2+} binding site, indicating that the metal ion is coordinated to two imidazole nitrogens from HisH126 and HisH128 and one oxygen from AspH124. A water molecule has been proposed to interact with Zn^{2+}, determining a tetrahedral coordination. Following these indications, we chose as reference compounds Zn-phthalocyanine, Zn-porphine, and Zn-heptanedionate. In Zn-phthalocyanine and Zn-porphine the metal ion coordinates four nitrogens belonging to pyrrolic rings. The structural unit of the Zn site in these compounds describes very well the bond of the metal ion with a histidine residue through the N^δ atom of the imidazole ring. In Zn-heptanedionate the first coordination shell around the absorber is composed by four oxygens and the higher shells contain carbon atoms in a configuration similar to that of the aspartic acid residue. In Fig. 1 we report the local structure of Zn in the described configurations.

The XAFS oscillations were extracted from the raw data with the AUTOBK program (Newville et al., 1993), using a linear function for the preedge region and a cubic spline to mimic the atomic background. In the inset of Fig. 2 we show the background subtracted XAFS function for sample 2 in order to illustrate the quality of the data. The main part of Fig. 2 reports the magnitude of the Fourier Transforms of the XAFS data, performed in the range 2.4–14 Å^{-1} with a k^1 weight. The first peak is due to the first coordination shell composed by O and/or N atoms, whereas the less intense peaks between 2 and 5 Å are due to the signal from the higher coordination shells, due to both single and multiple scattering contributions.

The data were analyzed with the FEFFIT program (Newville et al., 1995) using ab initio phase shifts generated with the FEFF 8.0 code (Ankudinov et al., 1998). A preliminary aspect of the data analysis consisted in the fitting of

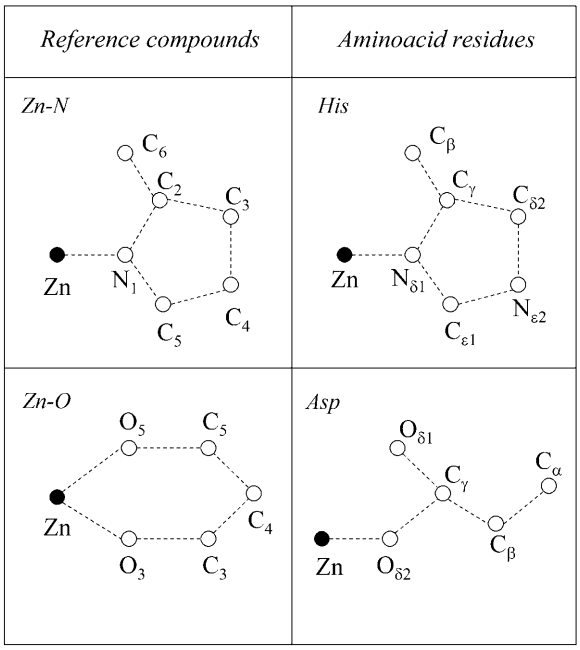

FIGURE 1 Sketch of the atomic structures considered in the analysis of the model compounds and of the amino acidic residues bound to Zn^{2+}. (*Top*) on the left the pyrrolic ring, the considered structural unit of Zn-phthalocyanine and Zn-porphine; on the right the imidazole of histidine. (*Bottom*) on the left the considered group of atoms of Zn-heptanedionate; on the right the side chain of aspartic acid.

the spectra of the reference compounds. The aim was twofold: on one hand to verify that, with the known structure as a starting point, the ab initio calculated scattering phase shifts allowed fits of the experimental data with reasonable structural parameters and, on the other, to determine which MS paths contribute significantly to the experimental signal.

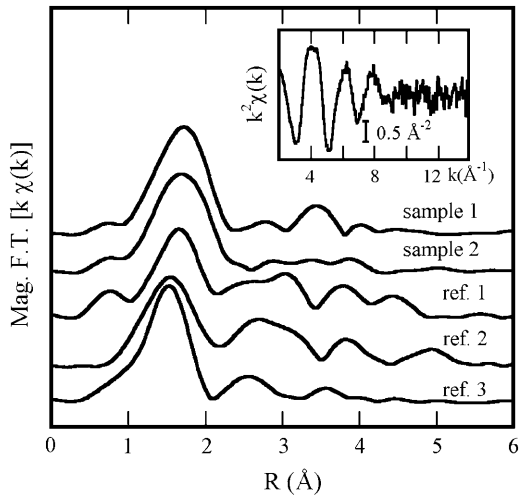

FIGURE 2 The magnitude of the Fourier transforms of the XAFS data for the two samples and three reference compounds; reference 1 is Zn-porphine, reference 2 is Zn-phthalocyanine, and reference 3 is Zn-heptanedionate. In the inset, the raw, background subtracted data for sample 2 are shown.

For all the reference compounds good fits were obtained. Best fitting structural parameters, which are in good agreement with the known values (Drabløs et al., 1999), are listed in Table 1. In particular the first shell Zn-O and Zn-N interatomic distances are within 0.04 Å of the published values for similar Zn coordination. In Fig. 3, we show, as an example, the fit for Zn-phthalocyanine together with all the significant contributions. The contributions are labeled by $\chi_n^{(i)}$, where i is a running index and n indicates the number of ''legs'' in the scattering path ($n = 2$ for a single scattering signal). The atomic configuration corresponding to each $\chi_n^{(i)}$ signal is listed in Table 1, using the atom labels indicated in Fig. 1. The fit of Zn-phthalocyanine was performed in the range $k = 2.4 - 12$ Å^{-1} and $R = 1.2 - 4$ Å with a total of 14 fitting parameters: the many-body amplitude reduction factor S_0^2, a common shift in the energy origin ΔE, and for each of the six paths a distance variation and a Debye Waller factor; the coordination numbers were kept fixed. We found that extending the analysis to the higher coordination shells was essential in order to improve the reliability of the local structural parameters of the first shell. In particular we found that, when analyzed in real space, some of the higher shell signals (both single scattering and MS) have a low distance tail which extends below the first shell peak.

As expected (Strange et al., 1987; Meneghini and Morante, 1998), MS paths have a significant amplitude in the presence of a ring structure bound to the metal. In fact, in

TABLE 1 Structural parameters obtained for the reference compounds

Zn-porphine			
Atomic paths	R (Å)	σ^2 (Å^2)	Path degeneracy
$\chi_2^{(1)}$ Zn-N_1	2.072(4)	0.0043(4)	4
$\chi_2^{(2)}$ Zn-$C_{2,5}$	3.112(5)	0.0038(7)	8
$\chi_2^{(3)}$ Zn-C_6	3.513(6)	0.0016(9)	4
$\chi_2^{(4)}$ Zn-$C_{3,4}$	4.5(4)	0.1(2)	8
$\chi_3^{(1)}$ Zn-N_1-$C_{2,5}$	3.26(3)	0.027(7)	16
$\chi_3^{(2)}$ Zn-N_1-$C_{3,4}$	4.5(2)	0.0060(7)	16
Zn-phthalocyanine			
Atomic paths	R (Å)	σ^2 (Å^2)	Path degeneracy
$\chi_2^{(1)}$ Zn-N_1	1.995(5)	0.00348(5)	4
$\chi_2^{(2)}$ Zn-$C_{2,5}$	3.021(8)	0.0059(9)	8
$\chi_2^{(3)}$ Zn-C_6	3.456(7)	0.0002(6)	4
$\chi_2^{(4)}$ Zn-$C_{3,4}$	4.44(1)	0.001(1)	8
$\chi_3^{(1)}$ Zn-N_1-$C_{2,5}$	3.39(5)	0.03(1)	16
$\chi_3^{(2)}$ Zn-N_1-$C_{3,4}$	4.27(6)	0.032(8)	16
Zn-heptanedionate			
Atomic paths	R (Å)	σ^2 (Å^2)	Path degeneracy
$\chi_2^{(1)}$ Zn-$O_{3,5}$	1.95(1)	0.0035(15)	4
$\chi_2^{(2)}$ Zn-$C_{3,5}$	3.17(7)	0.001(6)	4
$\chi_3^{(1)}$ Zn-$O_{3,5}$-$C_{3,5}$	3.24(6)	0.00(1)	8

The 1 σ error on the least significant figure is reported in brackets. For χ_3 path, the half-scattering pathlength is listed.

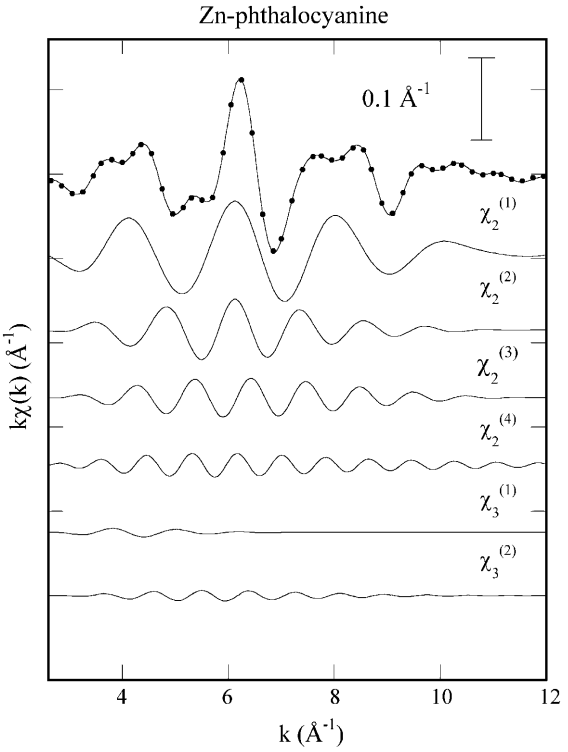

FIGURE 3 Fit of the XAFS spectrum of Zn-phthalocyanine. The top curve shows the inverse Fourier transform (*continuous line*) and its fit (*dots*); also shown are the six contributions labeled as described in the text.

Zn – phthalocyanine the analysis can be done up to a distance of 4.5 Å from Zn atom, and it is necessary to involve two MS paths to have a good fit, whereas in the case of Zn-heptanedionate (in which there are no ring structures) the signal is much less structured, not allowing the extraction of structural parameters beyond a distance of 3.5 Å. The two MS paths we found involve the first shell N/O atom and C atoms in the second and fourth coordination shells, as detailed in Table 1.

Zn-RC complexes

We now describe the analysis of the data relative to the two samples, starting with sample 2 (Zn/RC ratio equal to 0.9 ± 0.1, based on atomic absorption determination, see Materials and Methods). We recall that in Fig. 1 we depict the structure of the residues coordinating the metal ion in the RC (atoms are labeled according to the Protein Data Bank conventions) and we use the XRD determination by Axelrod et al. (2000) as a starting point of our analysis.

The contributions included in the fitting are described in the following in order of increasing distance from the Zn atom. We take the first coordination shell as composed by 4 atoms (2 O, 2 N). To reduce the number of fitting parameters, we grouped together the higher shell atoms in sets with similar distances from the absorber, in some cases making atom substitutions. In this way, we have identified three other coordination shells, and the corresponding single scattering signals. The second shell contains four C belonging to histidines ($C_{\varepsilon 1}$ and C_γ), a C and an O belonging to aspartic acid (C_γ, $O_{\delta 1}$). This shell is approximated with six C atoms at a distance, which is expected to be close to the Zn-C second shell distance obtained for Zn-phthalocyanine or Zn-porphine. The third shell is composed by two C atoms which are the two C_β of the histidines, and the corresponding distance is expected to be close to the Zn-C_6 in the pyrrolic ring. The fourth shell is composed by the two C and the two N atoms of the histidines ($C_{\delta 2}$, $N_{\varepsilon 2}$) and by a C of the aspartic acid (C_β), and was approximated by five C atoms. Finally, we have also included the two MS paths we have previously shown to be important in the study of Zn-porphine and Zn-phthalocyanine. In using the same χ_3 signals as in the reference compounds we make some approximations by exchanging certain atoms, as can be deduced from a comparison of Table 1 and Table 2. In particular, four of the twelve $\chi_3^{(1)}$ paths approximated by a Zn-N-C signal are in fact Zn-O-C (two paths) or Zn-O-O (two paths) and of the eight $\chi_3^{(2)}$ paths approximated by a Zn-N-C signal four are in

TABLE 2 Results of the fit for sample 2, compared to the distances deduced from XRD

Site of major affinity					
XAFS				XRD	
Atomic paths	R (Å)	σ^2 (Å^2)	Path degeneracy	Atomic configuration	$\langle R \rangle$
$\chi_2^{(1\_O)}$	1.98(3)	0.003(6)	2	Zn-O (H_2O); $-O_{\delta 2}$ (AspH124)	2.2
$\chi_2^{(1\_N)}$	2.11(3)	0.000(4)	2	Zn-$N_{\delta 1}$ (HisH126, HisH128)	2.2
$\chi_2^{(2)}$	3.07(3)	0.018(6)	6	Zn-C_γ, $-O_{\delta 1}$ (AspH124); Zn-C_γ (HisH126, HisH128); Zn-$C_{\varepsilon 1}$ (HisH126, HisH128)	3.1
$\chi_2^{(3)}$	3.48(4)	0.000(4)	2	Zn-C_β (HisH126, HisH128)	3.5
$\chi_2^{(4)}$	4.4(1)	0.00(1)	5	Zn-C_β (AspH124); Zn-$C_{\delta 2}$ (HisH126, HisH128); Zn-$N_{\varepsilon 2}$ (HisH126, HisH128)	4.3
$\chi_3^{(1)}$	3.12(4)	0.000(5)	12	Zn-$N_{\delta 1}$-$C_{\varepsilon 1,\gamma}$ (HisH126, HisH128) Zn-$O_{\delta 2}$-C_γ,$O_{\delta 1}$ (AspH124)	3.4
$\chi_3^{(2)}$	4.46(9)	0.00(2)	8	Zn-$N_{\delta 1}$-$C_{\delta 2}$,$N_{\varepsilon 2}$ (HisH126, HisH128)	4.4

The 1 σ error on the least significant figure is reported in brackets. For χ_3 path, the half-scattering pathlength is listed. The path degeneracies were kept fixed.

fact Zn-N-N. As theoretical signals we used the ones generated from the same cluster we built in the study of Zn-phthalocyanine after substituting the C_4 atom of pyrrole ring with the $N_{\varepsilon 2}$ atom.

The fit was performed in the range $k = 2.4 - 14$ Å^{-1} and $R = 1.1 - 4.2$ Å with a total of 16 fitting parameters: the many-body amplitude reduction factor S_0^2, a common shift in the energy origin ΔE, and for each of the seven paths a distance variation and a Debye Waller factor; the coordination numbers were kept fixed. The numerical results obtained are reported in Table 2 whereas the fit is reported in Fig. 4, along with the separate contributions. Also in this case we found that extending the analysis to the higher coordination shells was essential in order to improve the reliability of the local structural parameters of the first shell.

As can be noticed (see Table 2) we found a considerable (0.1 − 0.2 Å) contraction of the first shell distances compared to the XRD data. We have verified that this contraction does not depend on the analysis method: it is apparent in a simple comparison of the experimental data with a simulation based on the XRD determination (not shown). Similar differences have been reported when comparing local structures in metalloproteins determined by XAFS and by XRD at resolutions between 3.0 and 2.0 Å (Samar Hasnain and Strange, 2003). With no doubt the estimate obtained by XAFS is more precise and accurate, having a 1 σ error of only 0.03 Å.

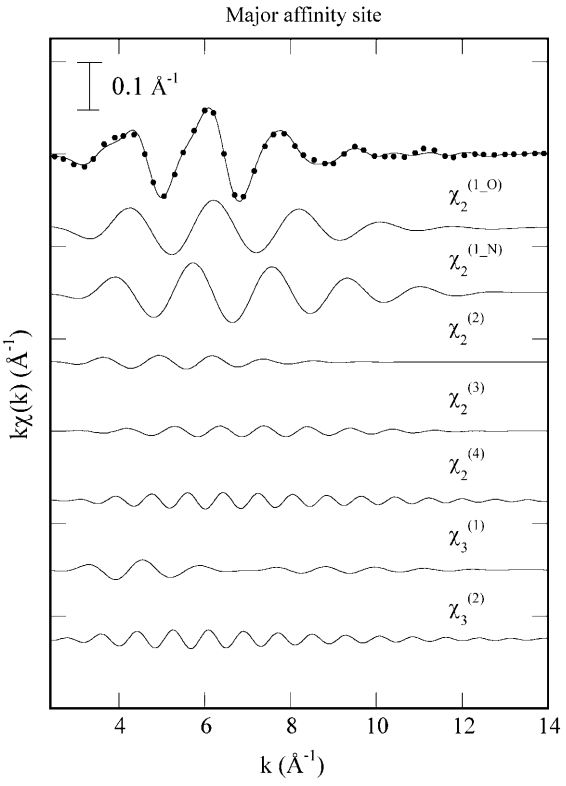

FIGURE 4 Fit of the XAFS spectrum of sample 2. The top curve shows the inverse Fourier transform (*continuous line*) and its fit (*dots*); also shown are the seven contributions labeled as described in the text.

For the higher coordination shells the path distances obtained are very similar to those which can be deduced from XRD, with the exception of the first MS path, for which there is a 0.3 Å discrepancy. Our best fitting structural parameters are in good agreement with the values found for similar Zn cluster in other proteins (Meneghini and Morante, 1998; Hough and Hasnain, 2003). The agreement of the higher shell interatomic distances with the XRD determination at the relatively high resolution of 2.5 Å implies an unexpected accuracy of the crystallographic work.

We now come to the analysis of sample 1, characterized by a Zn/RC ratio equal to 1.9 ± 0.2. As detailed under Materials and Methods, a Zn/RC stoichiometry close to two could be obtained reproducibly by incubating the RC with a four-times excess $ZnSO_4$ at two RC concentrations. Analysis of the complete gel chromatography elution profile in these preparations evidences a good separation between free and RC-bound Zn^{2+}, making it extremely unlikely that the stoichiometry found in sample 1 includes a contribution from free Zn ions. The reversibility of Zn^{2+} binding was demonstrated by equilibrium dialysis against a metal chelating resin (see Materials and Methods). The visible-NIR absorption spectrum of RC-Zn complexes characterized by ~2 Zn/RC (not shown) is essentially coincident with that of RC not incubated with Zn ions. In particular the spectrum does not reveal any alteration of the Q_y band of the bacteriochlorophyll dimer at 865 nm, indicating that no anomalous aggregation of the RC complexes has occurred after incubation even at relatively high metal concentrations. This absorption band, in fact, has been shown to respond with a sizeable blue shift to RC aggregation (Palazzo et al., 2004).

In Fig. 2, we see that the Fourier transform of the XAFS signal for this sample is very different compared to that of sample 2 in the region corresponding to the higher coordination shells. Control measurements, in which the signal of a Zn-PVA matrix, in the absence of RC, was acquired (not shown), further confirm the absence of free Zn ions in sample 1. Therefore we can reasonably expect that, besides the site of high affinity discussed in sample 2, there is at least another site of minor affinity. Although the occurrence of two or more lower affinity sites (partially occupied in sample 1) cannot be excluded a priori, we made the simplifying assumption of a single lower affinity site and attempted to extract the XAFS signal of this unknown site. Using the measured values of the Zn/RC ratio we determine the XAFS signal of this second Zn^{2+} site as:

$$\chi_{\text{site2}} = \frac{1.9\chi_{\text{exp}} - \chi_{\text{site1}}}{0.9},$$

where χ_{site1} and χ_{site2} are the XAFS functions relative to the two sites, of major and minor affinity respectively, and χ_{exp} is the XAFS function extracted from our data of sample 1.

The fundamental problem in analyzing χ_{site2} was that we had no preliminary indications about the local structure. However, it is reasonable to assume that Zn binds in the first

shell to N and O, and, since we already had precise information about these distances, we tried to fit the first shell using Zn-O and Zn-N theoretical signals. In a first step we left as free parameter the number of N and O atoms, with the constrain that the total number of first shell bonds was four; we found the best fit for three N and one O atoms. Having determined the composition of the first coordination shell, we proceeded in studying the second shell.

We reasonably expect the second shell to be composed by C atoms, since this is the case in all the probable residues. We verified that the only path which fits our data in the second shell is a Zn-C one, similar to that found in Zn-heptanedionate, with a distance (3.26 Å) which is considerably longer than that found in Zn-porphine or Zn-phthalocyanine; this strongly suggests that we can exclude the presence of C from a histidine residue. An exact determination of the numbers of carbon atoms in second shell was found to be impossible because of the large errors associated with this parameter when it was left free. The number of C atoms is taken constant at the value of three. In Fig. 5 and in Table 3 we show the results obtained from the fit.

XRD analysis of RC crystals soaked in $ZnSO_4$ containing mother liquor has revealed the existence of a single electron density peak largely exceeding the background level, identified as the Zn ion bound to the high affinity site (Axelrod et al., 2000). Axelrod et al. (2000) also observed a few other difference peaks, considerably lower than the major one, interpreted as anion or detergent binding sites. In principle additional binding sites could have been partially occupied also in the crystals examined by Axelrod et al. (2000) and could have contributed to the above-mentioned minor density peaks.

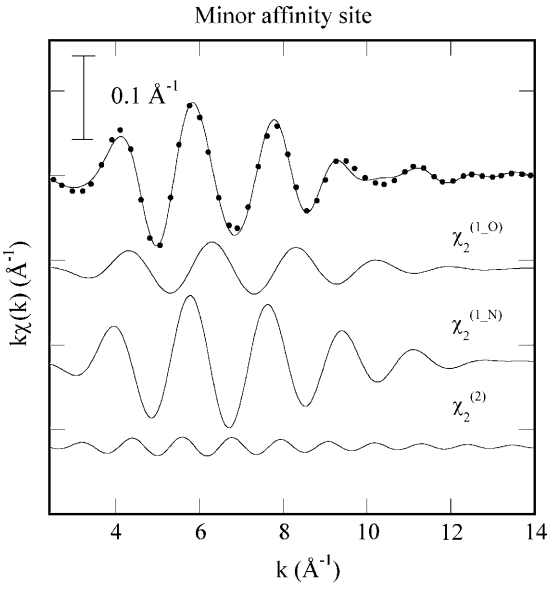

FIGURE 5 Fit of signal from the lower affinity site. The top curve shows the inverse Fourier transform (*continuous line*) and its fit (*dots*); also shown are the three contributions labeled as described in the text.

TABLE 3 Results of the fit of the minor affinity site

Site of minor affinity			
Atomic paths	R (Å)	σ^2 (Å^2)	Path degeneracy
$\chi_2^{(1\_O)}$	1.96(2)	0.000(3)	1
$\chi_2^{(1\_N)}$	2.10(5)	0.000(7)	3
$\chi_2^{(2)}$	3.26(4)	0.002(5)	3

The 1 σ error on the least significant figure is reported in brackets. The path degeneracies were kept fixed.

Since second shell analysis of the lower affinity binding site revealed by our investigation leads to exclude coordination to histidine residues, ligands providing the three N atoms of the first shell can be restricted to Gln, Asn, Lys, and Arg. Inspection of a database of Zn binding sites in proteins of known structure (http://tanna.bch.ed.ac.uk/cngroups.html), indicates a number of sites which include one or two Gln; Asn and Lys are less frequently present as donors of an N atom and only three binding sites contain one Arg residue. On this basis, we attempted to identify possible locations of the lower affinity binding site by searching for clusters of three N atoms belonging to Gln, Asn, Lys, or Arg residues lying on the hydrophilic surface of the RC protein. We discarded clusters in which the distance between two N atoms exceeds 7 Å as well as those containing two or more Arg residues. By interrogating the XRD structure of the RC (Protein Data Bank entry 1AIJ; Stowell et al., 1997) for clusters satisfying the above criterion, we found two groups (GlnH199-AsnH201-ArgH202 and AsnL199-ArgM267-LysH62) lying on the cytoplasmic hydrophilic portion and one on the periplasmic surface of the L subunit (GlnL264-LysL268-AsnL280). All three putative sites include an Arg and/or a Lys residue. Coordination of a metal ion by these amino acids is uncommon, requiring the deprotonation of the charged amino group of Lys and of guanidinium group of Arg, both characterized by typically high pK_a values. However it has been suggested that the coordinating ability of these groups can be strongly enhanced by the proximity of a His residue, which would act as a base, facilitating their deprotonation (Khangulov et al., 1998; Ferraroni et al., 2002). No His is present in the surroundings of the putative periplasmic site. At variance, a His residue is found in the proximity of ArgH202 and ArgM267-LysH62 of the two cytoplasmic sites (HisH204 and HisM145, respectively). In the latter, cluster coordination could be further facilitated by the presence of the carboxyl group of GluM263 (the O atoms of which being at 3 Å from the side chain N of LysH62). In the XRD structure of the RC determined in the presence of Zn^{2+} (Protein Data Bank entry 1DV6; Axelrod et al., 2000) a Cl^- is also detected at ~3–4 Å from the N atoms of the guanidinium group of ArgM267. Interestingly a chlorine anion is present at one of the Arg containing Zn binding sites documented by XRD (Ferraroni et al., 2002).

Finally, we recall that two Zn^{2+} binding sites have been recently located by XRD in the cytochrome bc_1 complex (Berry et al., 2000). Also in this integral protein complex, Zn^{2+} has been shown to inhibit electron and proton transfer (Link and von Jagow, 1995; Klishin et al., 2002) and both Zn^{2+} binding sites identified in the crystallographic structure have been considered as potential inhibitory sites (Berry et al., 2000).

CONCLUSIONS

X-ray absorption spectroscopy of stoichiometric Zn-RC complexes allows a clear-cut determination of the local structure of the high affinity Zn^{2+} binding site previously identified by x-ray diffraction at 2.5 Å resolution (Axelrod et al., 2000). Accurate analysis of the XAFS regions of the spectrum in terms of single and multiple scattering paths nicely fits, up to the fourth coordination shell, a Zn^{2+} binding cluster which consists of HisH126, HisH128, AspH124, and a water molecule. The coordination geometry obtained in the noncrystalline sample characterized by a Zn/RC ratio close to one reproduces well the one proposed on the basis of XRD data in RC crystals soaked in the presence of the metal and determines the first shell distances with an error equal to 0.03 Å. The first shell distances resulting from our study are considerably contracted in comparison with those determined by XRD.

At variance with what reported by Utschig et al. (1998) we found that incubation of RCs in the presence of a moderate stoichiometric excess of Zn over the protein, followed by gel filtration chromatography, results systematically in Zn-RC complexes characterized by Zn/RC ratios close to two. This strongly suggests that the high affinity site located by XRD is not the only Zn^{2+} binding site of the RC. Both RC-bound Zn ions can be removed by equilibrium dialysis against a metal chelating resin. The XAFS spectrum of one of such samples (Zn/RC $= 1.9 \pm 0.2$) is consistent with the existence of a new, lower affinity site which involves one O and three N, not belonging to a histidine residue. The possible contribution of the lower affinity binding site to inhibition of electron and/or proton transfer should be considered in functional studies performed in the presence of excess metal ion.

By interrogating the crystallographic structures of the RC we have proposed two possible locations of the second binding site at the cytoplasmic surface of the reaction center.

The authors thank P. Turina, B. A. Melandri, S. Ciurli, and C. Tomasini for useful discussions.

The financial support of MIUR of Italy is acknowledged by F.F. and G.V. (grant PRIN/2003 ''Bioenergetica: genomica funzionale, meccanismi molecolari ed aspetti fisiopatologici''; grant FIRB/2001 ''Meccanismi molecolari della fotosintesi''); and by G.P. (grant PRIN/2003 ''Nuovi biosensori basati su neurorecettori immobilizzati''). G.P. was supported by the Consorzio Interuniversitario per lo sviluppo dei Sistemi a Grande Interfase (CSGI-Firenze). F.F. was also supported by A. M. Contigliozzi and A. Contigliozzi. Financial support for measurements at ESRF were provided by INFM.

REFERENCES

Ädelroth, P., M. L. Paddock, L. B. Sagle, G. Feher, and M. Y. Okamura. 2000. Identification of the proton pathway in bacterial reaction centers: both protons associated with reduction of Q_B to Q_BH_2 share a common entry point. *Proc. Natl. Acad. Sci. USA.* 97:13086–13091.

Ädelroth, P., M. L. Paddock, A. Tehrani, J. T. Beatty, G. Feher, and M. Y. Okamura. 2001. Identification of the proton pathway in bacterial reaction centers: decrease of proton transfer rate by mutation of surface histidines at H126 and H128 and chemical rescue by imidazole identifies the initial proton donors. *Biochemistry.* 40:14538–14546.

Allen, J. P., G. Feher, T. O. Yeates, H. Komiya, and D. C. Rees. 1987a. Structure of the reaction center from *Rhodobacter sphaeroides* R-26: The cofactors. *Proc. Natl. Acad. Sci. USA.* 84:5730–5734.

Allen, J. P., G. Feher, T. O. Yeates, H. Komiya, and D. C. Rees. 1987b. Structure of the reaction center from *Rhodobacter sphaeroides* R-26: The protein subunits. *Proc. Natl. Acad. Sci. USA.* 84:6162–6166.

Allen, J. P., G. Feher, T. O. Yeates, D. C. Rees, J. Deisenhofer, H. Michel, and R. Huber. 1986. Structural homology of reaction centers from *Rhodopseudomonas sphaeroides* and *Rhodopseudomonas viridis* as determined by x-ray diffraction. *Proc. Natl. Acad. Sci. USA.* 83:8589–8593.

Ankudinov, A. L., B. Ravel, J. J. Rehr, and S. D. Conradson. 1998. Real space multiple-scattering calculation and interpretation of x-ray-absorption near-edge structure. *Phys. Rev. B.* 58:7565–7576.

Axelrod, H. L., E. C. Abresch, M. L. Paddock, M. Y. Okamura, and G. Feher. 2000. Determination of the binding site of the proton trasfer inhibitors Cd^{2+} and Zn^{2+} in bacterial reaction centers. *Proc. Natl. Acad. Sci. USA* 97:1542–1547.

Balabin, I. A., and J. N. Onuchic. 2000. Dynamically controlled protein tunneling paths in photosynthetic reaction centers. *Science.* 290:114–117.

Baxter, R. H. G., N. Ponomarenko, V. Šrajer, R. Pahl, K. Moffat, and J. R. Norris. 2004. Time-resolved crystallographic studies of light-induced structural changes in the photosynthetic reaction center. *Proc. Natl. Acad. Sci. USA.* 101:5982–5987.

Berry, E. A., Z. Zhang, H. Bellamy, and L. Huang. 2000. Crystallographic location of two Zn^{2+}-binding sites in the avian cytochrome bc_1 complex. *Biochim. Biophys. Acta.* 1459:440–448.

Bunker, G., E. A. Stern, R. A. Blankenship, and W. W. Parson. 1982. An x-ray absorption study of the iron site in bacterial photosynthetic reaction centers. *Biophys. J.* 37:539–551.

Chen, L. X., L. M. Utschig, S. L. Schlesselman, and D. M. Tiede. 2004. Temperature and light-induced structural changes in photosynthetic reaction center proteins probed by X-ray absorption fine structure. *J. Phys. Chem. B.* 108:3912–3924.

Ciatto, G., F. D'Acapito, F. Boscherini, and S. Mobilio. 2004. Treatment of EXAFS data taken in the fluorescence mode in non-linear conditions. *J. Synchrotron Radiat.* 11:278–283.

Crofts, A. R., and C. A. Wraight. 1983. The electrochemical domain of photosynthesis. *Biochim. Biophys. Acta.* 726:149–185.

Drabløs, F., D. G. Nicholson, and M. Rønning. 1999. EXAFS study of zinc coordination in bacitracin A. *Biochim. Biophys. Acta.* 1431:433–442.

Eisenberger, P., M. Y. Okamura, and G. Feher. 1982. The electronic structure of Fe^{2+} in reaction centers from *Rhodopseudomonas sphaeroides. Biophys. J.* 37:523–538.

Ermler, U., G. Fritzsch, S. K. Buchanan, and H. Michel. 1994. Structure of the photosynthetic reaction centre from *Rhodobacter sphaeroides* at 2.65 Å resolution: cofactors and protein-cofactor interactions. *Structure.* 2:925–936.

Feher, G., J. P. Allen, M. Y. Okamura, and D. C. Rees. 1989. Structure and function of bacterial photosynthetic reaction centres. *Nature.* 33: 111–116.

Ferraroni, M., S. Tilli, F. Briganti, W. R. Chegwidden, C. T. Supuran, K. E. Wiebauer, R. E. Tashian, and A. Scozzafava. 2002. Crystal structure of a zinc-activated variant of human carbonic anhydrase I, CA I Michigan

1: evidence for a second zinc binding site involving arginine coordination. *Biochemistry*. 41:6237–6244.

Filipponi, F., A. Di Cicco, and C. R. Natoli. 1995. X-ray-absorption spectroscopy and n-body distribution functions in condensed matter. I. Theory. *Phys. Rev. B*. 52:1–15.

Gerencsér, L., and P. Maroti. 2001. Retardation of proton transfer caused by binding of the transition metal ion to the bacterial reaction center is due to pK_a shifts of key protonatable residues. *Biochemistry*. 40:1850–1860.

Gray, K. A., J. W. Farchaus, J. Wachtveitl, J. Breton, and D. Oesterhelt. 1990. Initial characterization of site-directed mutants of tyrosine M210 in the reaction centre of *Rhodobacter sphaeroides*. *EMBO J*. 9:2061–2070.

Gunner, M. R. 1991. The reaction center protein from purple bacteria: structure and function. *Curr. Top. Bioenerg*. 16:319–367.

Hoff, A. J., and J. Deisenhofer. 1997. Photophysics of photosynthesis. Structure and spectroscopy of reaction centers of purple bacteria. *Phys. Rep*. 287:1–247.

Hough, M. A., and S. S. Hasnain. 2003. Structure of fully reduced bovine copper zinc superoxide dismutase at 1.15 Å. *Structure*. 11:937–946.

Khangulov, S. V., T. M. Jr. Sossong, D. E. Ash, and G. C. Dismukes. 1998. L-Arginine binding to liver arginase requires proton transfer to gateway residue His141 and coordination of the guanidinium group to the dimanganese (II,II) center. *Biochemistry*. 37:8539–8550.

Klishin, S. S., W. Junge, and A. Y. Mulkidjanian. 2002. Flash-induced turnover of the cytochrome bc_1 complex in chromatophores of *Rhodobacter capsulatus*: binding of Zn^{2+} decelerates likewise the oxidation of cytochrome b, the reduction of cytochrome c_1 and the voltage generation. *Biochim. Biophys. Acta*. 1553:177–182.

Koninsgsberger, D. C., and R. Prins. 1988. X-Ray Absorption: Principles, Applications, Techniques of EXAFS, SEXAFS and XANES. Wiley, New York.

Link, T. A., and G. von Jagow. 1995. Zinc ions inhibit the Q_P center of bovine heart mitochondrial bc_1 complex by blocking a protonatable group. *J. Biol. Chem*. 270:25001–25006.

McMahon, B. H., J. D. Müller, C. A. Wraight, and G. U. Nienhaus. 1998. Electron transfer and protein dynamics in the photosynthetic reaction center. *Biophys. J*. 74:2567–2587.

Meneghini, C., and S. Morante. 1998. The active site structure of tetanus neurotoxin resolved by multiple scattering analysis in x-ray absorption spectroscopy. *Biophys. J*. 75:1953–1963.

Newville, M., P. Livins, Y. Yacoby, E. A. Stern, and J. J. Rehr. 1993. Near-edge x-ray-absorption fine structure of Pb: a comparison of theory and experiment. *Phys. Rev. B*. 47:14126–14131.

Newville, M., B. Ravel, D. Haskel, J. J. Rehr, E. A. Stern, and Y. Yacoby. 1995. Analysis of multiple-scattering XAFS data using theoretical standards. *Physica B*. 208/209:154–155.

Okamura, M. Y., M. L. Paddock, M. S. Graige, and G. Feher. 2000. Proton and electron transfer in bacterial reaction centers. *Biochim. Biophys. Acta*. 1458:148–163.

Paddock, M. L., G. Feher, and M. Y. Okamura. 2000. Identification of the proton pathway in bacterial reaction centers: replacement of Asp-M17 and Asp-L210 with Asn reduces the proton transfer rate in the presence of Cd^{2+}. *Proc. Natl. Acad. Sci. USA*. 97:1548–1553.

Paddock, M. L., M. S. Graige, G. Feher, and M. Y. Okamura. 1999. Identification of the proton pathway in bacterial reaction centers: inhibition of proton transfer by binding of Zn^{2+} or Cd^{2+}. *Proc. Natl. Acad. Sci. USA*. 96:6183–6188.

Paddock, M. L., P. H. McPherson, G. Feher, and M. Y. Okamura. 1990. Pathway of proton transfer in bacterial reaction centers: replacement of serine-L223 by alanine inhibits electron and proton transfers associated with reduction of quinone to dihydroquinone. *Proc. Natl. Acad. Sci*. 87: 6803–6807.

Paddock, M. L., L. Sagle, A. Tehrani, J. T. Beatty, G. Feher, and M. Y. Okamura. 2003. Mechanism of proton transfer inhibition by Cd^{2+} binding to bacterial reaction centers: determination of the pK_A of functionally important histidine residues. *Biochemistry*. 42:9626–9632.

Palazzo, G., A. Mallardi, F. Francia, M. Dezi, G. Venturoli, M. Pierno, E. Vignati, and R. Piazza. 2004. Spontaneous emulsification of detergent solubilized reaction center: protein conformational changes precede droplets growth. *Phys. Chem. Chem. Phys*. 6:1439–1445.

Pascarelli, S., F. Boscherini, F. D'Acapito, J. Hrdy, C. Meneghini, and S. Mobilio. 1996. X-ray optics of a dynamical sagittal focussing monochromator on the GILDA beamline at the ESRF. *J. Synchrotron Radiat*. 3:147–155.

Poluektov, O. G., L. M. Utschig, S. Dalosto, and M. C. Thurnauer. 2003. Probing local dynamics of the photosynthetic bacterial reaction center with a cysteine specific spin label. *J. Phys. Chem. B*. 107:6239–6244.

Rehr, J. J., and R. C. Albers. 2000. Theoretical approaches to x-ray absorption fine structure. *Rev. Mod. Phys*. 72:621–654.

Samar Hasnain, S., and K. O. Hodgson. 1999. Structure of metal centres in proteins at subatomic resolution. *J. Synchrotron Rad*. 6:852–864.

Samar Hasnain, S., and R. W. Strange. 2003. Marriage of XAFS and crystallography for structure—function studies of metalloproteins. *J. Synchrotron Rad*. 10:9–15.

Stowell, M. H. B., T. M. McPhillips, D. C. Rees, S. M. Soltis, E. Abresch, and G. Feher. 1997. Light-induced structural changes in photosynthetic reaction center: implication for mechanism of electron-proton transfer. *Science*. 276:812–816.

Straley, S. C., W. W. Parson, D. C. Mauzerall, and R. K. Clayton. 1973. Pigment content and molar extinction coefficients of photochemical reaction centers from *Rhodopseudomonas sphaeroides*. *Biochim. Biophys. Acta*. 305:597–609.

Strange, R. W., N. J. Blackburn, P. F. Knowles, and S. Samar Hasnain. 1987. X-ray absorption spectroscopy of metal-histidine coordination in metalloproteins. *J. Am. Chem. Soc*. 109:7157–7162.

Takahashi, E., and C. A. Wraight. 1992. Proton and electron transfer in the acceptor quinone complex of *Rhodobacter sphaeroides* reaction centers: characterization of site-directed mutants of the two ionizable residues, GluL212 and AspL213, in the Q_B binding site. *Biochemistry*. 31:855–866.

Utschig, L. M., Y. Ohigashi, M. C. Thurnauer, and D. M. Tiede. 1998. A new metal-binding site in photosynthetic bacterial reaction centers that modulates Q_A to Q_B electron transfer. *Biochemistry*. 37:8278–8281.

Woodbury, N. W., and J. P. Allen. 1995. The pathway, kinetics, and thermodynamics of electron transfer in wild type and mutant reaction centers of purple nonsulfur bacteria. *In* Anoxygenic Photosynthetic Bacteria. R. E. Blankenship, M. T. Madigan, and C. E. Bauer, editors. Kluwer Academic Publishers, Dordrecht, The Netherlands. 527–557.